Instabilities in the Linear Sb Atom Chain of the New Binary Antimonide $Ti_{11-x}Sb_{8-y}$

Svilen Bobev[†] and Holger Kleinke*[,‡]

Los Alamos National Laboratory, Los Alamos, New Mexico, 87545, and Department of Chemistry, University of Waterloo, Waterloo, ON, Canada N2L 3G1

Received May 6, 2003. Revised Manuscript Received June 25, 2003

The new binary antimonide $Ti_{11-x}Sb_{8-y}$ was prepared from directly reacting the elements in stoichiometric ratios, either by melting the reaction mixture in an arc furnace or by annealing it in a resistance furnace above 1000 °C. $Ti_{11-x}Sb_{8-y}$ is a nonstoichiometric compound with a small phase range that cannot be prepared with the idealized Ti:Sb ratio of 11:8. $Ti_{10.84(3)}Sb_{7.74(1)}$ crystallizes in the $Cr_{11}Ge_8$ type, isostructural with $(Zr,V)_{11}Sb_8$: space group *Pnma*, lattice dimensions $a = 1462.28(9)$ pm, $b = 559.72(4)$ pm, $c = 1764.4(1)$ pm, $V = 1.4441(2)$ nm^3 ($Z = 4$). One can describe this type as an intergrowth of distorted fragments of the NiAs and W_5Si_3 types. In addition to the dominating heteronuclear Ti−Sb bonds, the structure of $Ti_{11-x}Sb_{8-y}$ comprises several homonuclear Ti−Ti and Sb−Sb bonding interactions. Short bonds of alternating 276 and 284 pm occur in a linear nonclassical chain of mainly Sb atoms (i.e., 87% Sb and 13% Ti). According to our experiments, the incorporation of Ti atoms into this chain, which consists solely of Sb atoms with shorter interatomic distances than those in the ternary Zr−V antimonide, is necessary for the formation of this compound to balance the mismatch of bond length and strength in this chain.

Introduction

New, mostly metal-rich binary pnictides and chalcogenides of the group 4 metals are continuously being found, the majority of which occurred in previously unknown structure types. Examples of the past few years include Ti_5Sb_8,[1] Ti_9Se_2,[2] $Ti_{11}Se_4$,[3] $Zr_{11}Sb_{18}$,[4] Zr_3Te,[5] Zr_2Te,[6] Hf_7P_4,[7] Hf_2Te,[8] and Hf_3Te_2.[9] The structures of all these compounds exhibit both bonding metal−metal and metal−nonmetal/metalloid interactions. In contrast to the metal−metal bonds, typically no contacts exist between the anionic components, i.e., the chalcogen or pnicogen atoms (with the exception of the two antimonides with intermediate Sb−Sb interactions of 310−325 pm). On the other hand, the ternary antimonides $(Zr,V)_{13}Sb_{10}$[10] (new type), $(Zr,V)_{11}Sb_8$[11] ($Cr_{11}Ge_8$[12] type), and (Zr,Ti)Sb[13] (new type) contain short Sb−Sb bonds in linear Sb atom chains. It was shown that the Sb−Sb interactions in these chains are best described as half bonds, and the Sb atoms are best described as being in the −2 state, albeit the bond lengths (between 280 and 290 pm) correspond to classical single bond distances. Related linear chains of Sb atoms with larger interatomic distances (>306 pm) were discussed in a detailed review published in 2000 to comprise nonclassical ("hypervalent") bonding with an ideal electron count of 7 valence-electrons per atom.[14]

Here, the related binary antimonide of the idealized stoichiometry $Ti_{11}Sb_8$ ($Cr_{11}Ge_8$ type, isostructural with $(Zr,V)_{11}Sb_8$) will be discussed. We preliminarily reported on $Ti_{11-x}Sb_{8-y}$ by exhibiting a poster during a conference;[15] also, a ternary variant $Ti_{11}(Sn,Sb)_8$ was published by Kauzlarich et al.[16] that interestingly does not show any Ti incorporation in the linear Sn/Sb atom chain.

Experimental Section

Synthesis. All experiments were started from elemental titanium and antimony as purchased in powder form (titanium, ALFA AESAR, −100 mesh, 99.4%; antimony, MERCK, 99.8%). $Ti_{11-x}Sb_{8-y}$ can be prepared by arc-melting pressed pellets of 2.8 mmol Ti and 2.0 mmol Sb on a water-cooled copper hearth in an argon atmosphere. The X-ray powder diffraction pattern of the ground reaction product(s) consisted only of the reflections of the new phase, whereas analogous

* To whom correspondence should be addressed. E-mail: kleinke@uwaterloo.ca.
[†] Los Alamos National Laboratory.
[‡] University of Waterloo.

(1) Zhu, Y.; Kleinke, H. *Z. Anorg. Allg. Chem.* **2002**, *628*, 2233.
(2) Weirich, T. E.; Simon, A.; Pöttgen, R. *Z. Anorg. Allg. Chem.* **1996**, *622*, 630−634.
(3) Weirich, T. E.; Ramlau, R.; Simon, A.; Hovmoeller, S.; Zou, X. *Nature (London)* **1996**, *382*, 144−146.
(4) Elder, I.; Lee, C.-S.; Kleinke, H. *Inorg. Chem.* **2002**, *41*, 538−545.
(5) Harbrecht, B.; Leersch, R. *J. Alloys Compd.* **1996**, *238*, 13−17.
(6) Örlygsson, G.; Harbrecht, B. *Inorg. Chem.* **1999**, *38*, 3377−3383.
(7) Kleinke, H.; Franzen, H. F. *Angew. Chem., Int. Ed. Engl.* **1996**, *35*, 1934−1936.
(8) Harbrecht, B.; Conrad, M.; Degen, T.; Herbertz, R. *J. Alloys Compd.* **1997**, *255*, 178−182.
(9) Abdon, R. L.; Hughbanks, T. *Angew. Chem., Int. Ed. Engl.* **1994**, *33*, 2328−2330.
(10) Kleinke, H. *Chem. Commun. (Cambridge)* **1998**, 2219−2220.
(11) Kleinke, H. *J. Mater. Chem.* **1999**, *9*, 2703−2708.
(12) Israiloff, P.; Völlenkle, H.; Wittmann, A. *Monatsh. Chem.* **1974**, *105*, 1387−1404.
(13) Kleinke, H. *J. Am. Chem. Soc.* **2000**, *122*, 853−860.
(14) Papoian, G. A.; Hoffmann, R. *Angew. Chem., Int. Ed.* **2000**, *39*, 2408−2448.
(15) Kleinke, H. *Z. Kristallogr. Suppl.* **1999**, *16*, 42.
(16) Kim, H.; Olmstead, M. M.; Chan, J. Y.; Canfield, P. C.; Fisher, I. R.; Henning, R. W.; Schultz, A. J.; Kauzlarich, S. M. *J. Solid State Chem.* **2001**, *157*, 225−232.

10.1021/cm034328d CCC: $25.00
Published on Web 07/29/2003

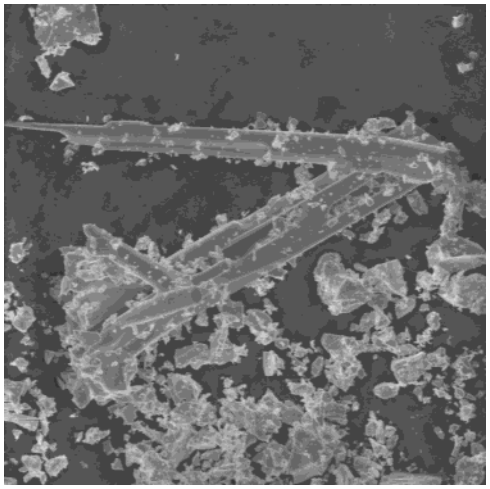

Figure 1. SEM picture of needle-shaped $Ti_{11-x}Sb_{8-y}$ crystals. Width of the image area is 250 μm.

reactions with slightly different starting Ti:Sb ratios, i.e., 1.5:1 and 1.3:1, led to mixtures of two antimonides, namely Ti_5Sb_3/$Ti_{11-x}Sb_{8-y}$ and $Ti_{11-x}Sb_{8-y}$/TiSb, respectively. In all cases, the weight loss during arc melting (<5 wt %) stems from partial vaporization of antimony (boiling point 1587 °C), as proven by EDX investigations of the condensed vapor. Thus, the stoichiometries of the products of the arc-melted mixtures were slightly more Ti-rich than the starting Ti:Sb ratios, namely 1.45, 1.57, and 1.39, respectively. This indicates the Ti:Sb ratio of the new phase as being between 1.39 and 1.57.

Subsequently, $Ti_{11-x}Sb_{8-y}$ was synthesized at 1100 °C in quantitative yields by a solid-state reaction in a tantalum container sealed under argon, starting from 0.4 mmol Ti_5Sb_3[17] and 0.8 mmol TiSb[18]

$$0.2\ Ti_5Sb_3 + 0.4\ TiSb \rightarrow \text{“}Ti_{1.4}Sb\text{”} \equiv Ti_{11-x}Sb_{8-y}$$

Both known antimonides, Ti_5Sb_3 and TiSb, typically form platelike crystals, and $Ti_{11-x}Sb_{8-y}$ tends to crystallize in needle-shaped crystals, as evident in the solid-state reaction products (Figure 1). Only titanium and antimony were detected in the energy-dispersive X-ray analysis using an electron microscope (CAM-SCAN, CS 4DV) with an additional EDX device (detector, NORAN Instruments), i.e., no impurities (e.g., coming from the reaction container) were present. The Ti:Sb ratio of selected needlelike crystals of the solid-state reaction was averaged to be 59(1):41 at % (i.e., 1.44:1 Ti:Sb). Control measurements of TiSb and Ti_5Sb_3 indicated that the EDX results are very reliable in the Ti−Sb system.

Structure Determination. A single-crystal data collection was performed on a needlelike crystal using an IPDS diffractometer (STOE). The crystal was taken from the arc-melting reaction of 2.8 mmol Ti and 2 mmol Sb. The positions of 5000 reflections with $I > 6\sigma(I)$ were used to refine the lattice dimensions. The data were corrected for Lorentz and for polarization effects. A numerical absorption correction carried out was based on measured crystal faces. The space group *Pnma* was chosen based on the systematic extinctions; lowering the symmetry by removing the inversion center (space group $Pn2_1a$) led to strong correlations between the sites that are equivalent in *Pnma*, but to no improvement of the residual values.

The structure solution[19] pointed toward adoption of the $Cr_{11}Ge_8$ type. The refinement of this model with Ti atoms on the Cr sites and Sb atoms on the Ge sites converged smoothly to satisfying residual values (e.g., $R(F) = 0.0314$). Treating all crystallographically independent sites (nine Ti and seven Sb) as fully occupied (ideal stoichiometry “$Ti_{11}Sb_8$”) led to displacement parameters for Ti6-7 and Sb6-7 that were slightly higher than twice the average of the other atom sites. Therefore, the occupancy factors of the former sites were refined resulting in significant deviations from full occupancy in the cases of Ti6 (occupancy, 75(1) %), Ti7 (82(1) %), and Sb7 (92.1(3) %), whereas the occupancy factor of the Sb6 position was refined to 100% within one standard deviation. Interestingly, these two Ti sites and, even more so, the Sb6 site display high displacement parameters in the recently published $Ti_{11}(Sn,Sb)_8$ as well, while the “Sb7” position in the ternary compound, postulated to be a mixed Sn/Sb site, is inconspicuous. Furthermore, no irregular thermal parameters were found in $(Zr,V)_{11}Sb_8$.

Table 1. Crystallographic Data for $Ti_{10.84(3)}Sb_{7.73(1)}$

chemical formula	$Ti_{10.84(3)}Sb_{7.73(1)}$
formula weight [g/mol]	1460
T of measurement [K]	295
λ [pm]	71.073
space group	*Pnma*
ρ_{calcd} [g/cm^3]	6.72
a [pm]	1462.28(9)
b [pm]	559.72(4)
c [pm]	1764.4(1)
V [nm^3]	1.4441(2)
Z	4
μ [cm^{-1}]	197.6
$R(F_o)^a/R_w(F_o^2)^b$	0.027/0.036

^{a} $R(F_o) = \sum||F_o|-|F_c||/\sum|F_o|$. ^{b} $R_w(F_o^2) = [\sum[w(F_o^2 - F_c^2)^2]/\sum[w(F_o^2)^2]]^{1/2}$

This structure model yielded a formula of “$Ti_{10.56(2)}Sb_{7.84(1)}$”, i.e., a Ti:Sb ratio of 1.347(3), which, however, is not in agreement with the phase analyses discussed above. Supposing a mixed Ti/Sb occupancy on the so-called “Sb7” site, which cannot be distinguished from Sb defects by X-rays, resulted in a Ti:Sb ratio of 13.3(5):86.7 on this site and the formula $Ti_{10.84(3)}Sb_{7.73(1)}$ (Ti:Sb ratio = 1.402(4)), and a final $R(F) = 0.0267$. Correspondingly, an elemental analysis (atomic absorption spectroscopy, AAS) of the seemingly single-phase product of the solid-state reaction of the starting ratios of 1.4:1 yielded a Ti:Sb ratio of 1.42(2), thereby confirming the above-mentioned refined formula of $Ti_{10.84(3)}Sb_{7.73(1)}$. It is therefore concluded that the “Sb7” site is mixed occupied by Ti and Sb, in addition to the two deficient Ti sites. The formula therefore could be written in a more informative, albeit complex, way as $Ti_{11-\delta}(Ti_{0.13}Sb_{0.87})_1Sb_7$, to indicate both the presence of deficient Ti sites and of one mixed Ti/Sb site. Crystallographic details of this model are given in Table 1, and atomic positions with occupancy factors and equivalent displacement parameters are shown in Table 2.

A second single-crystal study was carried out with a crystal of the single-phase sample of the initial composition “$Ti_{1.4}Sb$”, which was prepared at 1100 °C to check for ordering phenomena. The results of this study did not differ significantly from the first one in any respect; the final formula was determined to be $Ti_{10.88(6)}Sb_{7.74(1)}$ (Ti:Sb = 1.406(7)), which is within the standard deviations of the same composition, despite the different Ti:Sb ratios (while the starting ratios were equivalent, the final ratios were not because of vaporization ofonly Sb in the arc melter). Therefore, the phase range of $Ti_{11-x}Sb_{8-y}$ is assumed negligible.

Neutron Studies. To verify the structure model of mixed Ti/Sb occupancies on the “Sb7” position, a neutron diffraction experiment was carried out on the time-of-flight, High-Pressure Preferred Orientation (HIPPO) neutron diffractometer at the Manuel Lujan Jr. Neutron Scattering Center at Los Alamos National Laboratory. The instrument utilizes chilled water as a moderator and has a short primary flight path distance (moderator to sample) of 9.0 m for the sake of higher neutron flux at the expense of resolution. Approximately 2 g of finely ground sample was loaded in a vanadium can and backscattering data were collected at room temperature for roughly 2 h. The resolution and d-spacing range for the

(17) Berger, R. *Acta Chem. Scand.* **1977**, *31A*, 889−890.
(18) Nowotny, H.; Pesl, J. *Monatsh. Chem.* **1951**, *82*, 336−343.
(19) Sheldrick, G. M. *SHELXTL Version 5.12*; Reference Manual, Siemens Analytical X-ray Systems, Inc: Madison, WI, 1996.

Table 2. Positional and Displacement Parameters of $Ti_{10.84(3)}Sb_{7.73(1)}$

atom	site	*x*	*y*	*z*	U_{eq}/pm^2	occupancy
Sb1	4c	0.29577(7)	1/4	0.30250(5)	71(2)	1
Sb2	4c	0.43936(8)	1/4	0.51761(5)	65(2)	1
Sb3	4c	0.08212(7)	1/4	0.19467(5)	71(2)	1
Sb4	4c	0.23033(8)	1/4	0.90905(5)	113(2)	1
Sb5	4c	0.01601(8)	1/4	0.73966(6)	120(2)	1
Sb6	4c	0.04852(8)	1/4	0.43805(6)	218(3)	1
"Sb7"	8d	0.28753(5)	0.0036(2)	0.10813(4)	116(2)	0.867(5) Sb, 0.133 Ti
Ti1	4c	0.4332(2)	1/4	0.1921(1)	97(5)	1
Ti2	4c	0.1257(2)	1/4	0.0401(1)	89(6)	1
Ti3	4c	0.2013(2)	1/4	0.7494(2)	76(5)	1
Ti4	4c	0.3663(2)	1/4	0.6627(1)	80(6)	1
Ti5	4c	0.2475(2)	1/4	0.4669(1)	94(6)	1
Ti6	4c	0.3822(3)	1/4	0.9922(2)	180(1)	0.75(1)
Ti7	4c	0.0432(3)	1/4	0.5911(2)	200(1)	0.82(1)
Ti8	8d	0.06186(13)	0.0042(3)	0.87923(8)	69(3)	1
Ti9	8d	0.36578(12)	0.0082(3)	0.82343(9)	78(4)	1

backscattering detector banks are about 0.4% and 0.12 Å < *d* < 4.8 Å, respectively.

Starting from the structure model obtained from the single-crystal X-ray study, the structure refinement was done using the GSAS[20] software for Rietveld refinement with default neutron scattering lengths and absorption cross-sections. Final refinement cycles involved 14 parameters including background (power series function with 6 terms), peak shape, scaling factor, unit cell, and isotropic thermal parameters for all atoms, and occupancy factors for "Sb7", with residual factors of $R_P = 0.0214$ and $wR_P = 0.0144$. "Sb7" was refined as being mixed occupied by Sb and Ti, resulting in 63(2)% Sb and 37% Ti. In contrast to the X-ray experiment, large differences are to be expected between a model with mixed Ti/Sb occupancies and a model with Sb deficiencies, as the scattering lengths of Sb and Ti have different signs. Treating the "Sb7" site as an Sb-deficient position in an alternative refinement led to an unreasonably small occupancy factor of 0.41(2) % (i.e., a Ti:Sb ratio of 10.56:6.82 = 1.55) without significant changes in the residual factors. It is thus concluded that the model of mixed Ti/Sb occupancies on "Sb7" is the correct one, as it shows the best correlation of analytical data, X-ray, and neutron diffraction.

Calculations of the Electronic Structure. Semiempirical calculations were performed using the *tight binding* extended Hückel approximation,[21,22] solving the eigenvalue problem on a set of 48 *k* points. The Hückel parameters were taken from earlier work on TiSb.[13] In addition, the band structure of the structure model $^1_\infty[Ti_7Sb_2]$ was calculated in order to model the Sb substructure of the linear "Sb7" chain.

Physical Property Measurements. Temperature-dependent resistance measurements were carried out on a needlelike crystal contacted along the long axis between 300 and 10 K. Magnetic susceptibility measurements were performed on a ground bulk sample at 1 T in the temperature range of 1.8 to 300 K on a Quantum Design MPMS SQUID magnetometer. The data were corrected for the diamagnetic atom cores. Low field measurements were carried out (at 0.01 T) to check for any transitions, e.g., stemming from superconductivity. No anomalies were found, however.

Results and Discussion

Crystal Structure. For simplicity, the structure will be described based on fully occupied atomic sites without consideration of the deficiencies and mixed occupancies. A striking structure motif is a column of Ti atoms, centered by Sb atoms. These columns **A** consist of face-condensed defect square antiprisms $Ti_7\square_1$ that include a linear chain of "Sb7" atoms. This motif is reminiscent of the W_5Si_3 type, which comprises chains of face-condensed square antiprisms filled with a linear Si atom chain. The motifs **A** are densely packed parallel to the *b* axis, whereas the voids are filled with (distorted) fragments of the TiSb structure (NiAs type) (Figure 2), i.e., face-sharing $TiSb_6$ octahedra (and fragments thereof, namely $TiSb_5\square_1$). Altogether, the structure of $Ti_{11-x}Sb_{8-y}$ can be regarded as an intergrowth of fragments of the W_5Si_3 and NiAs types, a description that also holds for the structures of $M_{13}Sb_{10}$, isostructural $M_{11}Sb_8$ (M = Zr, V), and (to a lesser extent) (Zr,Ti)Sb.

The two symmetry-inequivalent chains of the NiAs fragments are shown in Figure 3. As a consequence of face-sharing, linear Ti atom chains form along the *b* axis, with distances of alternating 275 and 284 pm in the chain of Ti8-centered Sb_6 octahedra and 271 and 289 pm in the chain of the Ti9-centered defect $Sb_5\square_1$ "octahedra".

Besides the fact that all metal sites are occupied by a single atom kind, namely titanium, $Ti_{11-x}Sb_{8-y}$ also differs in the condensation of the channels **A** and thus

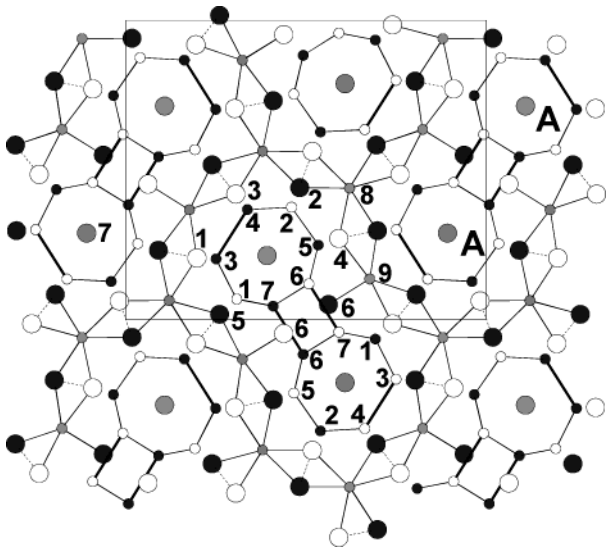

Figure 2. Projection of the structure of "$Ti_{11}Sb_8$" along [010]. Horizontal: *c* axis. Small circles, Ti; large circles, Sb. The different heights of the atoms are reflected in different shading. Thick lines: Ti−Ti distances *d* < 300 pm. Dotted lines: Sb−Sb around 336 pm. The W_5Si_3 and NiAs fragments are emphasized.

(20) Larson, A. C.; von Dreele, R. B. *GSAS−General Structure Analysis System*,; Los Alamos National Laboratory: Los Alamos, NM, 2000.

(21) Hoffmann, R. *J. Chem. Phys.* **1963**, *39*, 1397−1412.

(22) Whangbo, M.-H.; Hoffmann, R. *J. Am. Chem. Soc.* **1978**, *100*, 6093−6098.

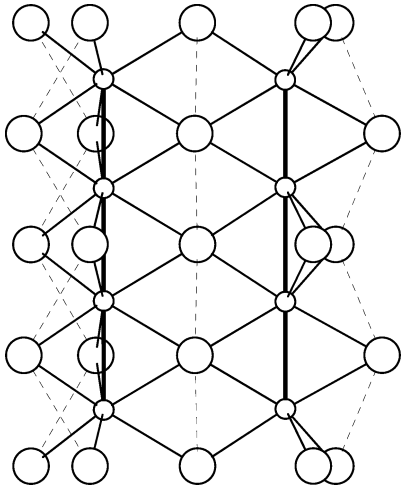

Figure 3. The $^1_\infty[Ti8Sb_6]$ and $^1_\infty[Ti9Sb_5\square_1]$ chains. Small circles, Ti; large circles, Sb.

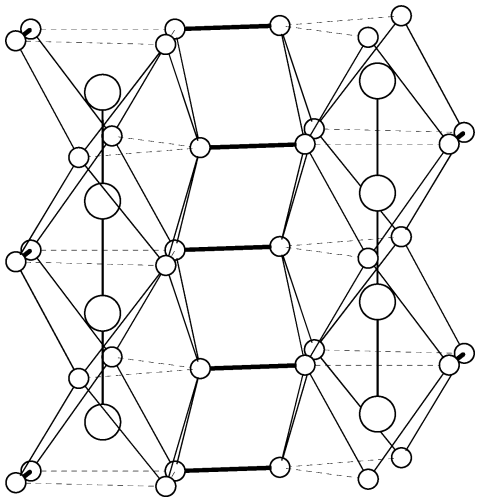

Figure 4. The $^1_\infty[Ti_7(Ti,Sb)_2]_2$ double chain. Small circles, Ti; large circles, "Sb7". Thick solid lines between the Ti atoms: distances d < 300 pm; thin solid lines, 300 pm < d < 360 pm; dashed lines, 360 pm < d < 400 pm.

in the M:Sb ratio from $M_{13}Sb_{10}$. Whereas in the latter case, the columns **A** occur as single columns, they are interconnected via Ti6−Ti7 bonds to double chains **AA** in the structure of $Ti_{11-x}Sb_{8-y}$ (Figure 4), i.e., topologically equivalent to the $W_{8/2}Si_{2/2}$ columns of the W_5Si_3 structure.

It is noted that the Ti sites Ti6 and Ti7 are the deficient ones, and comparable sites (that connect two columns **A**) are not found in $M_{13}Sb_{10}$. Furthermore, the shortest Ti−Sb bonds of 265 and 266 pm are Ti7−Sb5 and Ti6−Sb4. These bonds are unusually short, the shortest Ti−Sb bonds of all binary Ti antimonides, and shorter than the sum of the single bond radii (e.g., Pauling's single bond radii: $r_{Ti} + r_{Sb}$ = 132 pm + 139 pm = 271 pm[21]).

The ideal formula can be deduced from the double chain $(Ti_7Sb_2)_2$ being surrounded by 12 Ti8 atoms, which connect three motifs **AA**, and 12 Ti9 atoms that connect two **AA,** and 12 Sb atoms to be $1/2[(Ti_7Sb_2)_2Ti_{12/3}Ti_{8/2}Sb_{12}] = Ti_{11}Sb_8$. An analogous formulation for $M_{13}Sb_{10}$ gives $(M_7Sb_2)M_{6/3}M_{8/2}Sb_7Sb_{2/2} = M_{13}Sb_{10}$. On a higher structural hierarchy, the structure motifs **A** form (distorted) triangular 3^6 nets in $Ti_{11-x}Sb_{8-y}$ and square-triangular 3^2434 nets in $M_{13}Sb_{10}$. For more details refer to the original publication that compares $M_{13}Sb_{10}$ and $M_{11}Sb_8$.[11]

Electronic Structure. *Ti−Ti Interactions.* As expected for a metal-rich pnictide, the structure of $Ti_{11-x}Sb_{8-y}$ exhibits numerous bonding metal−pnicogen and metal−metal contacts. In addition to the Ti6−Ti7 interactions (d = 278 pm) mentioned above, short, presumably bonding, Ti−Ti contacts (271−289 pm) are located parallel to the b axis in the NiAs fragments as well as in the ac plane, namely in the $Ti_7\square_1$ square antiprisms ($d_{Ti3-Ti4}$ = 286 pm). These Ti−Ti distances are in part shorter than those in elemental titanium (hexagonal closed packed modification: bonds of 289 and 295 pm) and in Ti_5Sb_3 (284−299 pm), yet still longer than Ti−Ti single bonds (about 264 pm).

Ti−Sb Interactions. The Ti−Sb distances in $Ti_{11-x}Sb_{8-y}$ vary from 265 to 315 pm, thereby exhibiting a larger range than the bonds in both Ti_5Sb_3 (271−295 pm) and TiSb (283 pm). The defects of the Ti6−7 sites occur with distinct anisotropies in the displacement parameters of Ti6−7 and Sb4−6, with the latter atoms taking part in short Ti6−Sb and/or Ti7−Sb bonds. These bonds are 5−6 pm shorter than the shortest Ti−Sb bond in Ti_5Sb_3 of 271 pm, which is equivalent to the sum of the single bond radii of Ti and Sb (271 pm).

Sb−Sb Interactions. In contrast to other metal-rich pnictides (and chalcogenides), several pnicogen−pnicogen contacts are observed in $Ti_{11-x}Sb_{8-y}$. The atoms Sb1−5 all take part in Sb zigzag chains with interatomic distances between 335 and 339 pm, which are comparable to the longer bond in elemental antimony with a length of 336 pm. Such distances are often found in transition metal antimonides, and are typically weakly bonding.[11,23−25]

In addition, the "Sb7" atoms form linear channels with interatomic distances of alternating 276 and 284 pm, which are shorter than the shortest bond in the element (291 pm). The different lengths of these two bonds likely have a sterical reason: the shorter bond is capped by three Ti atoms, and the longer bond is capped by four. Sb−Sb distances between 280 and 290 pm are typical for classical two-electron-two-center bonds (single bonds), as comparisons with polyantimonides such as the Zintl compound KSb (283 and 285 pm)[26] show. However, such a bonding situation would require sp^3 hybridization, resulting in the formation of a zigzag or helical chain as in KSb or elemental tellurium, rather than a linear chain. Extended Hückel calculations of the model structures of linear infinite Zr_7Sb_2 chains revealed that these Sb−Sb bonds in $(Zr,V)_{13}Sb_{10}$ and $(Zr,V)_{11}Sb_8$ are best described as ("hypervalent") delocalized one-electron-two-center σ bonds. Whereas this formalism explains the linearity of the chain, the distances of 280 and 288 pm in $Zr_{7.5}V_{5.5}Sb_{10}$ are definitely shorter than expected: a typical Sb−Sb bond with a bond order of 1/2 would be about 310 pm.[13,14,27,28]

(23) Kleinke, H. *Inorg. Chem.* **1999**, *38*, 2931−2935.
(24) Kleinke, H. *Chem. Soc. Rev.* **2000**, *29*, 411−418.
(25) Kleinke, H. *Inorg. Chem.* **2001**, *40*, 95−100.
(26) Hönle, W.; von Schnering, H.-G. *Z. Kristallogr.* **1981**, *155*, 307−314.
(27) Bolloré, G.; Ferguson, M. J.; Hushagen, R. W.; Mar, A. *Chem. Mater.* **1995**, *7*, 2229−2231.
(28) Kleinke, H. *Eur. J. Inorg. Chem.* **1998**, 1369−1375.

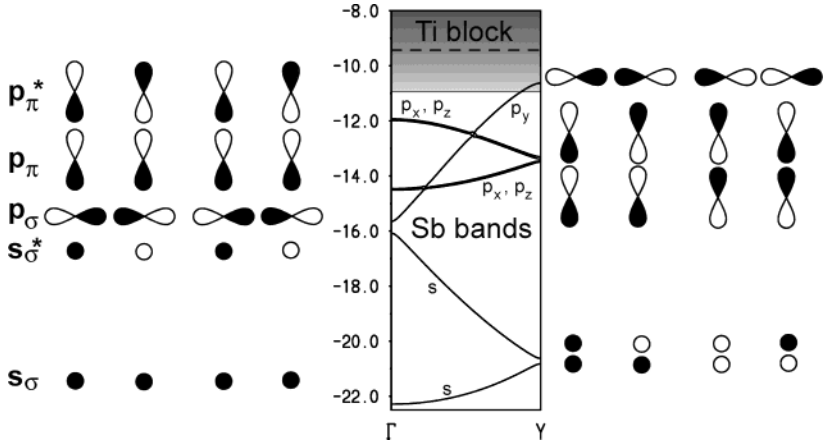

Figure 5. Schematic band structure of a $^1_\infty[Ti_7Sb_2]$ chain. Dashed horizontal line is Fermi level.

The same formalism can be applied to the Sb−Sb bonds of the idealized $^1_\infty[Ti_7Sb_2]$ chain (Figure 5; treating "Sb7" as a pure Sb site): seven bands of the two Sb atoms occur below the (partly filled) block dominated by Ti-*d* bands, namely the s_σ, s_σ*, both p_π and both p_π*, and the p_σ band, which are all completely filled. Then, seven valence-electrons are assigned to each Sb atom, rendering it Sb^{-2}. In a more simplifying picture,[29] one may regard all electrons except for those in the p_z orbitals as lone pairs, for the other orbitals are full and do not contribute to the region around the Fermi level.

Because of matrix effects, the "Sb7"−"Sb7" bonds are even shorter in $Ti_{11-x}Sb_{8-y}$, by 4 pm each (276 and 284 pm), compared to $M_{13}Sb_{10}$, because the surrounding metal atoms (Ti) are significantly smaller than in $Zr_{7.5}V_{5.5}Sb_{10}$, where these metal sites are predominantly Zr, namely 92% Zr and 8% V (cf., e.g., Pauling's single bond radii: $r_{Ti} = 132$ pm, $r_{Zr} = 145$ pm, $r_V = 122$ pm[21]). Although the second distance of 284 pm corresponds to a typical Sb−Sb single bond, the former (276 pm) is even shorter than the formal Sb−Sb double bond of 277 pm found in a distibene.[30] Thus, if judged by the bond lengths, this linear chain would contain alternating a double bond and a single bond, i.e., an averaged bond order of 1.5. In contrast to this, the electronic structure calculation shows that the two bonds exhibit each a bond order of (averaged) $^1/_2$. It is thus concluded that the defects in the Sb chain of $Ti_{11-x}Sb_{8-y}$ (i.e., partial replacement of "Sb7" by Ti) are a consequence of the otherwise too short interatomic distances, reducing the severe mismatch between bond length and order, because the resulting Ti−Sb distances of averaged 280 pm are in the common range for Ti−Sb bonds as discussed above.

Mixed occupancies of transition metal atoms and Sb atoms were observed before, albeit with other metal atoms in ternary compounds, e.g., mixed Ni/Sb occupancies in Hf_6NiSb_2,[31] and a number of different M/Sb occupancies in $Zr_5M_{0.5}Sb_{2.5}$ (M = Fe, Co, Ni)[32] and $Hf_{10}M_xSb_{6-x}$ with M = V, Cr, Mn, Fe, Co, Ni, and Cu.[33] These mixed occupancies may be understood as mixed anionic sites, for the most electropositive elements, Zr and Hf, are the major components, and can thus reduce both the *3d* metal as well as Sb. In the latter cases, which are variants of the W_5Si_3 type, the site mixed occupied with the M and Sb atoms forms a linear equidistant chain, quite comparable to the "Sb7" chain in $Ti_{11-x}Sb_{8-y}$. As $Ti_{11-x}Sb_{8-y}$, $Hf_{10}M_xSb_{6-x}$ does not exist without any M atoms in the linear chain, but in contrast to $Ti_{11-x}Sb_{8-y}$, it cannot be formed as a pure binary, i.e., with Hf atoms in the linear chain. $Ti_{11-x}Sb_{8-y}$ stands out in this class, as it exhibits mixed occupancies between the cationic component, Ti, and the anionic one, Sb.

The W_5Si_3 type is typically adopted by silicides and germanides, an observation indicating that the group 14 elements readily participate in such "hypervalent" chains. This also may explain why mixed Sn/Sb occupancies as in $Ti_{11}(Sn,Sb)_8$ are preferred over mixed Ti/Sb occupancies in these linear chains. Exceptions are the tellurides $M_xK_4Te_3$ (M = Ca, Sr),[34] which can be considered as electron-precise compounds $(M^{+2})_{0.5}(K^{+1})_4(Te^{-1})(Te^{-2})_2$, each Te^{-1} forming two one-electron-two-center bonds with expected lengths of above 300 pm.

DOS and COHP Curves. Figure 6 depicts the densities of states (DOS, left) and selected crystal orbital overlap populations (COOP,[35] middle and right). Excluded are the Sb-*s* peaks, which occur below the energy window shown. The lower peak in the DOS, situated between −16 and −11 eV, is dominated by Sb-*p* states; however, significant amounts of Ti states are filled in this range as well, as a consequence of the covalent character of the Ti−Sb bonds. The peak starting at −11 eV is mainly of Ti-*d* character, and overlaps slightly with the lower peak. The Fermi level (dashed horizontal line) cuts close to a local minimum through the Ti-*d* peak.

Only bonding states are filled in the cases of the Ti−Ti and Ti−Sb interactions. The curves shown were obtained by totaling those interactions over all bonds of these kinds in the unit cell, as listed in Table 3. A comparison of the Ti−Ti and Ti−Sb COOP curves

(29) Papoian, G.; Hoffmann, R. *J. Am. Chem. Soc.* **2001**, *123*, 6600−6608.
(30) Cowley, A. H.; Norman, N. C.; Pakulski, M.; Bricker, D. L.; Russell, D. H. *J. Am. Chem. Soc.* **1985**, *107*, 8211−8218.
(31) Kleinke, H. *J. Alloys Compd.* **1998**, *270*, 136−141.
(32) Kwon, Y. U.; Sevov, S. C.; Corbett, J. D. *Chem. Mater.* **1990**, *2*, 550−556.
(33) Kleinke, H.; Ruckert, C.; Felser, C. *Eur. J. Inorg. Chem.* **2000**, 315−322.
(34) Schewe-Miller, I.; Böttcher, P. *J. Alloys Compd.* **1992**, *183*, 98−108.
(35) Hughbanks, T.; Hoffmann, R. *J. Am. Chem. Soc.* **1983**, *105*, 3528−3537.

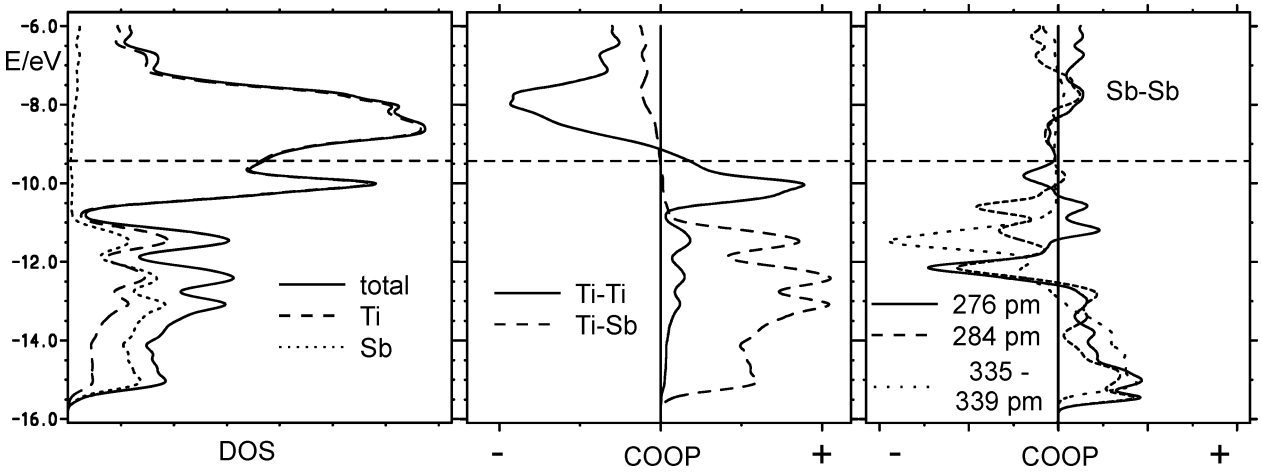

Figure 6. Densities of states (left) and selected COOP curves (middle and right) of idealized $Ti_{11}Sb_8$. Dashed horizontal line: Fermi level.

Table 3. Selected Interatomic Distances [pm] of $Ti_{10.84(3)}Sb_{7.73(1)}$

bond	length	no.	bond	length	no.
Ti1−Sb1	280.0(3)		Ti2−Sb4	277.2(3)	
Ti1−Sb6	284.8(3)		Ti2−Sb3	280.1(3)	
Ti1−Sb7	293.9(3)	2×	Ti2−Sb2	290.9(3)	
Ti1−Sb3	295.5(3)		Ti2−Sb2	298.3(1)	2×
Ti1−Sb5	301.5(1)	2×	Ti2−Sb7	299.0(3)	
Ti1−Ti9	328.6(3)	2×	Ti2−Ti8	328.9(3)	2×
Ti1−Ti7	333.6(2)	2×			
			Ti4−Sb2	277.4(3)	
Ti3−Sb5	271.5(3)		Ti4−Sb5	278.5(3)	
Ti3−Sb4	284.8(3)		Ti4−Sb7	282.9(3)	2×
Ti3−Ti4	285.7(4)		Ti4−Ti3	285.7(4)	
Ti3−Sb7	287.3(2)	2×	Ti4−Sb3	295.27(9)	2×
Ti3−Sb1	295.15(9)	2×	Ti4−Ti9	314.2(3)	2×
Ti3−Ti9	305.3(3)	2×	Ti4−Ti8	325.8(3)	2×
Ti3−Ti8	336.1(3)	2×			
			Ti6−Sb4	266.2(4)	
Ti5−Sb7	292.4(2)	2×	Ti6−Sb6	272.6(4)	
Ti5−Sb2	294.9(3)		Ti6−Ti7	277.5(6)	
Ti5−Sb6	295.1(3)		Ti6−Sb7	282.8(3)	2×
Ti5−Sb1	297.3(3)		Ti6−Sb6	312.6(2)	2×
Ti5−Sb4	299.2(1)	2×	Ti6−Ti9	328.0(4)	2×
Ti5−Ti9	334.3(3)	2×			
			Ti8−Ti8	275.2(4)	
Ti7−Sb5	265.2(3)		Ti8−Sb2	282.6(2)	
Ti7−Sb6	270.1(3)		Ti8−Ti8	284.5(4)	
Ti7−Ti6	277.5(6)		Ti8−Sb3	285.6(2)	
Ti7−Sb7	287.0(4)	2×	Ti8−Sb1	286.2(2)	
Ti7−Sb6	314.5(2)	2×	Ti8−Sb4	287.0(2)	
Ti7−Ti9	329.2(4)	2×	Ti8−Sb5	290.0(2)	
Ti7−Ti1	333.6(2)	2×	Ti8−Sb2	290.1(2)	
			Ti8−Ti4	325.8(3)	
Ti9−Ti9	270.7(4)		Ti8−Ti2	328.9(3)	
Ti9−Sb6	278.4(2)		Ti8−Ti3	336.1(3)	
Ti9−Sb1	279.4(2)				
Ti9−Sb3	279.8(2)		Sb7−Sb7	275.9(2)	
Ti9−Sb5	281.0(2)		Sb7−Sb7	283.8(2)	
Ti9−Sb4	283.5(2)				
Ti9−Ti9	289.0(4)				
Ti9−Ti3	305.3(3)				
Ti9−Ti4	305.3(3)				
Ti9−Ti6	328.0(4)				
Ti9−Ti1	328.6(3)				
Ti9−Ti7	329.2(4)				
Ti9−Ti5	334.3(3)				

implies the greater importance of the heteronuclear Ti−Sb interactions, which are optimized, as the transition between bonding and antibonding states occurs directly at the Fermi level. On the other hand, the Ti−Ti interactions would increase with an increase of the valence-electron concentration, as more bonding states would become filled.

The Sb−Sb interactions may be divided into three different groups; the averages thereof are shown in the left part of Figure 6. These are the two short bonds within the linear chain (276 and 284 pm), and the longer ones within the NiAs-like fragments (335−339 pm). All of these interactions have some antibonding states filled, and exhibit nonbonding states at the Fermi level. That they are overall of bonding character, i.e., more bonding than antibonding states are filled, can be taken from the calculated Mulliken overlap populations (MOPs):[36] these are 0.44 electrons for the shortest bond, 0.31 for the bond of 284 pm, and averaged 0.06 for the bonds around 335 pm. We calculated a MOP of 0.65 for the Sb−Sb single bonds of KSb, using the same Hückel parameters for Sb. Thus, the MOP values for the Sb−Sb interactions of the linear chain (averaged 0.37) are in agreement with the model of half bonds, compared to 0.65 for the full bond. Similar values were obtained for the linear chains of $(Zr,V)_{13}Sb_{10}$ (0.36), $(Zr,V)_{11}Sb_8$ (0.34),[11] and (Zr,Ti)Sb (0.38 electrons per bond).[13]

Physical Properties. The significant amount of densities of states prevalent at the Fermi level is indicative of metallic properties. Metallic character reflects itself in increasing electrical resistance with increasing temperature and small temperature-independent positive magnetic susceptibility (Pauli paramagnetism), stemming from the itinerant electrons. The experimentally determined electrical resistance and magnetic susceptibility are shown in Figure 7. Both curves are typical for metallic materials.

Summary

$Ti_{11-x}Sb_{8-y}$ is a new nonstoichiometric compound with a negligible phase range. It forms the $Cr_{11}Ge_8$ structure type, which is reminiscent of W_5Si_3- and NiAs-related fragments. In addition to two Ti-deficient positions, one site is mixed occupied by (mainly) Sb and Ti atoms. This latter site forms a linear chain with short interatomic distances of alternating 276 and 284 pm that inhibit a pure Sb position: these Sb−Sb bonds would be half bonds, but are shorter than single bonds in known

(36) Mulliken, R. S. *J. Chem. Phys.* **1955**, *23*, 2343−2346.

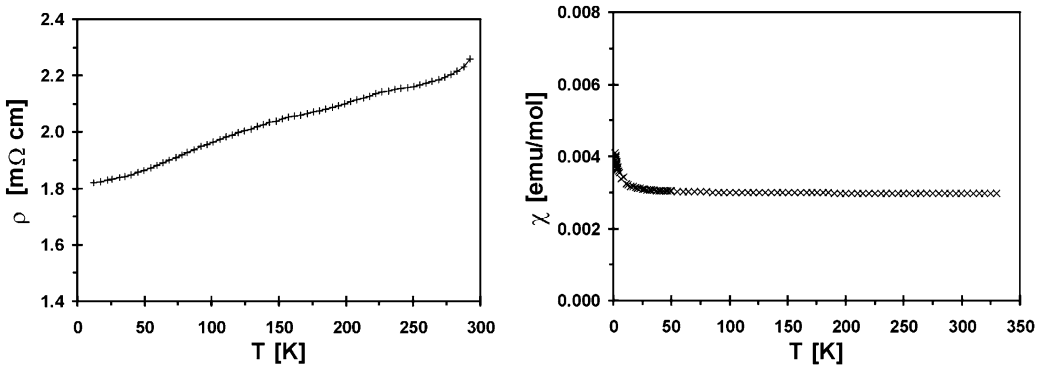

Figure 7. Specific electrical resistivity (left) and magnetic suceptibility (right) of $Ti_{11-x}Sb_{8-y}$.

polyantimonides. Replacing Sb in part by Ti atoms is required to reduce the tension, as Ti−Sb bonds of 280 pm are within the standard range. These Ti/Sb mixed occupancies are quite special, as they occur between the cationic and the anionic components.

Such linear Sb chains were known before, albeit with interatomic distances usually above 300 pm; related earlier examples found in our group exhibit Sb−Sb distances of 280−290 pm. Whereas mixed occupancies between early transition metal atoms and antimony are scarce, perhaps the most similar situation occurs in $Hf_{10}VSb_5$, an ordered variant of the W_5Si_3 type, wherein the linear chain consists of 50% V and 50% Sb atoms, with interatomic distances of 280 pm.

In addition to the prevalent Ti−Sb bonds, bonding homonuclear interactions of both possible kinds, Ti−Ti and Sb−Sb, contribute to the stability of $Ti_{11-x}Sb_{8-y}$. As predicted by the band structure calculations, $Ti_{11-x}Sb_{8-y}$ is a metallic material and exhibits Pauli paramagnetism.

Acknowledgment. This work was initiated at the FB Chemie of the University of Marburg (Germany), in particular supported by the group of Prof. B. Harbrecht, the Analytic Division, and Prof. J. Pebler. Current financial support from NSERC, CFI, OIT (Ontario Distinguished Researcher Award for H.K.), the Province of Ontario (Premier's Research Excellence Award for H.K.), and the Canada Research Chair program (CRC for H.K.) is appreciated. We are indebted to Dr. D. Williams (LANL/LANSCE-12) for his help with collecting the powder neutron diffraction data.

Supporting Information Available: One X-ray crystallographic file in CIF format. This material is available free of charge via the Internet at http://pubs.acs.org.

CM034328D